Geological Survey of Canada
Open File 8882

# AI-ENABLED REMOTE SENSING DATA INTERPRETATION FOR GEOTHERMAL RESOURCE EVALUATION AS APPLIED TO THE MOUNT MEAGER GEOTHERMAL PROSPECTIVE AREA, BRITISH COLUMBIA

Z. Chen[1], S.E. Grasby[1], C. Deblonde[1], and X. Liu[1]

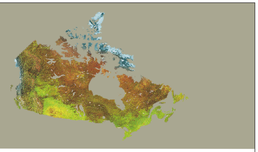

## Abstract

The objective of this study is to search for features and indicators from the identified geothermal resource sweet spot in the south Mount Meager area that are applicable to other volcanic complexes in the Garibaldi Volcanic Belt. A Landsat 8 multi-spectral band dataset, for a total of 57 images ranging from visible through infrared to thermal infrared frequency channels and covering different years and seasons, were selected. Specific features that are indicative of high geothermal heat flux, fractured permeable zones, and groundwater circulation, the three key elements in exploring for geothermal resource, were extracted. The thermal infrared images from different seasons show occurrence of high temperature anomalies and their association with volcanic and intrusive bodies, and reveal the variation in location and intensity of the anomalies with time over four seasons, allowing inference of specific heat transform mechanisms. Automatically extracted linear features using AI/ML algorithms developed for computer vision from various frequency bands show various linear segment groups that are likely surface expression associated with local volcanic activities, regional deformation and slope failure. In conjunction with regional structural models and field observations, the anomalies and features from remotely sensed images were interpreted to provide new insights for improving our understanding of the Mount Meager geothermal system and its characteristics. After validation, the methods developed and indicators identified in this study can be applied to other volcanic complexes in the Garibaldi, or other volcanic belts for geothermal resource reconnaissance.

## MMVC geothermal prospects and Geological Background

Mount Meager Volcanic Complex (MMVC) is a Quaternary volcanic massif that overlies on a post-Miocene erosion surface of crystal basement (Lewis and Souther, 1978) at the north end of Garibaldi Volcanic Belt (GVB) that stretches from the south on the U.S boarder to the north at the Bridge River volcanic cones. The MMVC has been the focus of geothermal research and exploration for a half century (Jessop, 2008). Other than MMVC, there has been limited geothermal research conducted in GVB given the remoteness and difficulty in access. Previous exploration has outlined the potential high temperature geothermal resource prospects and demonstrated that the southern Meager Creek geothermal reservoir is a fractured crystalline basement consisting of metamorphic rocks and quartz monzonite plutons. Subsequent production tests confirmed the presence of a permeable zone that defines the fractured reservoir, although the obtained water flow rate did not justify a commercial power plant (GeothermamEx Inc., 2004).

| Image type | Spectral band | Wavelength (μm) | Sensor | Description | Resolution (m) | Dataset A (Fall) | Note |
|---|---|---|---|---|---|---|---|
| Level-1 | B1 | 0.43 - 0.45 | OLI | Visible | 30 | LC08_L1TP_048025_20181019_20181031_01_T1 | Land Surface Temperature (LST) calculation and feature extraction |
| | B2 | 0.450 - 0.51 | OLI | Visible | 30 | | |
| | B3 | 0.53 - 0.59 | OLI | Visible | 30 | | |
| | B4 | 0.64-0.67 | OLI | Red | 30 | | |
| | B5 | 0.85-0.88 | OLI | Near Infrared (NIR) | 30 | | |
| | B6 | 1.57 - 1.65 | OLI | Shorte ave Infrared | 30 | | |
| | B7 | 2.11 - 2.29 | OLI | Shorte ave Infrared | 30 | | |
| | B10 | 10.60-11.19 | TIRS | Thermal Infrared (TIRS) 1 | 100m | | |
| | B11 | 11.50-12.51 | TIRS | Thermal Infrared (TIRS) 2 | 100m | | |
| Look | B4,5,6,10 | varies | OLITIRS | Multi-spectral | 30-100 | LC08_L1TP_048025_20140125_20170307_01_T1 | Feature extraction |
| | B4,5,6,10 | varies | OLITIRS | Multi-spectral | 30-100 | LC08_L1TP_048025_20140906_20170303_01_T1 | |
| | B4,5,6,10 | varies | OLITIRS | Multi-spectral | 30-100 | LC08_L1TP_048025_20150112_20170302_01_T1 | |
| | B4,5,6,10 | varies | OLITIRS | Multi-spectral | 30-100 | LC08_L1TP_048025_20170202_20170218_01_T1 | |
| | B4,5,6,10 | varies | OLITIRS | Multi-spectral | 30-100 | LC08_L1TP_048025_20170829_20170914_01_T1 | |
| | B4,5,6,10 | varies | OLITIRS | Multi-spectral | 30-100 | LC08_L1TP_048025_20170914_20170928_01_T1 | |
| | B4,5,6,10 | varies | OLITIRS | Multi-spectral | 30-100 | LC08_L1TP_048025_20180715_20180730_01_T1 | |
| | B4,5,6,10 | varies | OLITIRS | Multi-spectral | 30-100 | LC08_L1TP_048025_20180816_20180829_01_T1 | |
| | B4,5,6,10 | varies | OLITIRS | Multi-spectral | 30-100 | LC08_L1TP_048025_20181019_20181031_01_T1 | |
| | B4,5,6,10 | varies | OLITIRS | Multi-spectral | 30-100 | LC08_L1TP_048025_20181206_20181211_01_T1 | |
| | B4,5,6,10 | varies | OLITIRS | Multi-spectral | 30-100 | LC08_L1TP_048025_20190123_20190205_01_T1 | |
| | B4,5,6,10 | varies | OLITIRS | Multi-spectral | 30-100 | LC08_L1TP_048025_20191225_20200110_01_T1 | |

Table 1. Landsat 8 parameters of the data sets used in this study. Data were downloaded from USGS Earth Resources Observation and Science (EROS) Center. https://earthexplorer.usgs.gov/.

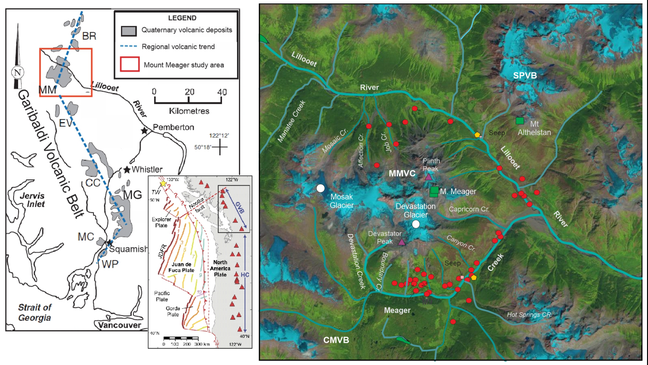


Figure 1. Map showing location of Mount Meager Volcanic Complex (MMVC) and the Garibaldi Volcanic Belt in western Canada (modified from Stewart, et al., 2002). BR (Bridge River), CC (Mt. Cayley), EV (Elaho Valley), MG (Mt. Garibaldi), MC (Mountain Creek), MM (Mt. Meager), WP (Watts Point). (Insert from Mullen and Weis, 2015).




Figure 2. A composite colour Landsat 8 image of the study area (Red box in Fig. 1) showing location of geothermal wells (red dots), hot springs (yellow pentagon), and major drainage system (blue lines).

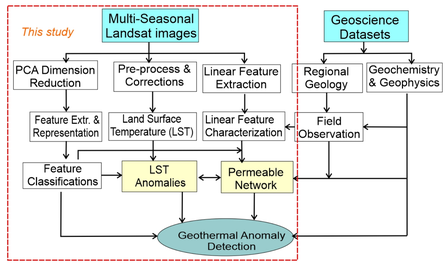


Figure 3. A flow chart showing the major components and interrelationship among various elements of this study (red box). Principal Component Analysis (PCA) was used for dimension reduction, K-means clustering method for feature classification, and Hough Transformation (HT) for linear feature detection. Land Surface Temperature (LST) were converted from Lansat 8 images (Table 1) using established method and workflow (Qin, 2011 and Darger, et al., 2019).

Table 2. Correlation coefficients matrix of the 9 multi-spectral bands of Landsat 8 images acquired on 2018-10-19 showing highly correlated image bands, particularly in visible and thermal infrared bands.

| Corr. Coef. | Band 1 | Band 2 | Band 3 | Band 4 | Band 5 | Band 6 | Band 7 | Band 10 | Band 11 |
|---|---|---|---|---|---|---|---|---|---|
| Band 1 | 1 | 0.9984 | 0.9889 | 0.9795 | 0.8824 | -0.2072 | -0.1199 | -0.5302 | -0.5347 |
| Band 2 | 0.9984 | 1 | 0.9948 | 0.9882 | 0.9006 | -0.1742 | -0.0868 | -0.4951 | -0.4988 |
| Band 3 | 0.9889 | 0.9948 | 1 | 0.9979 | 0.9277 | -0.1111 | -0.0244 | -0.4333 | -0.4361 |
| Band 4 | 0.9795 | 0.9882 | 0.9979 | 1 | 0.9414 | -0.058 | 0.0278 | -0.388 | -0.3902 |
| Band 5 | 0.8824 | 0.9006 | 0.9277 | 0.9414 | 1 | 0.1593 | 0.1911 | -0.1478 | -0.1534 |
| Band 6 | -0.2072 | -0.1742 | -0.1111 | -0.058 | 0.1593 | 1 | 0.9681 | 0.7636 | 0.769 |
| Band 7 | -0.1199 | -0.0868 | -0.0244 | 0.0278 | 0.1911 | 0.9681 | 1 | 0.6806 | 0.6919 |
| Band 10 | -0.5302 | -0.4951 | -0.4333 | -0.388 | -0.1478 | 0.7636 | 0.6806 | 1 | 0.9981 |
| Band 11 | -0.5347 | -0.4988 | -0.4361 | -0.3902 | -0.1534 | 0.769 | 0.6919 | 0.9981 | 1 |

## Methods & Workflow

Geological interpretation of remote sensing data is challenge because of: 1) multiple data sets from multi-spectral channels, and multiple collections in different seasons and years, and by different missions; 2) redundancy in similar, but different images resulted from overlapped physical responses in various spectral bands and repeated data acquisitions; 3) obscured and indirect relationship between features from images and surface/subsurface geology. Advanced image processing techniques and ML algorithms were used to reduce data redundancy and extract relevant features, and to eliminate subjectivity and improve efficiency in data processing and interpretation (Figure 3). Principal component analysis was used for dimension reduction and highlighting special subtle features, K-means clustering for feature classification, and Hough transformation for linear feature extraction. Land surface temperature conversion and geothermal heat flux mapping were conducted to outline surface temperature anomalies.

Post-processing, including labelling classes from unsupervised K-means clustering analysis using verified features from previous exploration, was performed to analyse identified anomalies, aggregate various intermediate products to visualize the location and intensity of geothermal anomalies, and to associate various linear segment groups with regional structural trends and local volcanic events. Confirmed anomalies were then integrated with field observations and geophysical data to highlight the areas for further study.

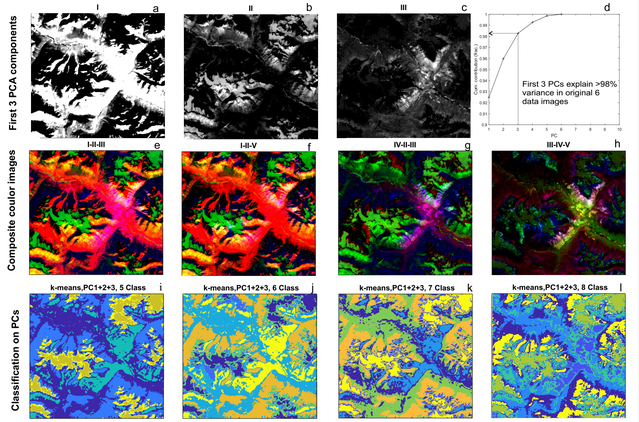


Fig. 4 Images showing first three PCs (a, b and c) of the orthogonal transformed linear combinations of the original images in the 9 bands (Table 1), which represents >98% of variance in the original data set (d); PC composite colour images from different combinations of PCs (e to h), and theme classification of different classes (i to l) for data interpretations.

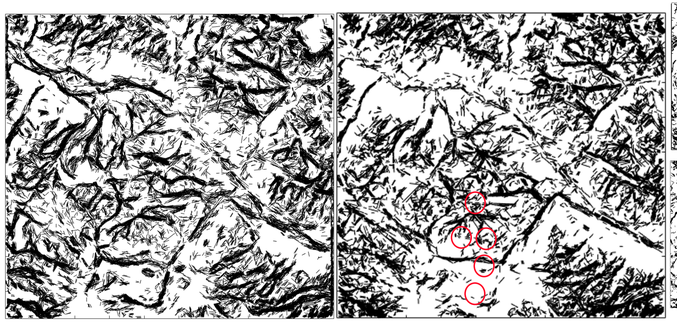


Fig. 5 Stacked linear segment maps from 12 thermal infrared image data sets acquired from 2014 to 2019 (Left) and from a single acquisition of 9 multi-spectral image bands (2018-10-19) (right) showing the similarities and differences in the characteristics of extracted linear features. The TIR images shows features closely related with thermal anomaly boundaries, while linear features from a signal multi-spectral are comprehensive, including topographical, vegetation and thermal boundaries, depicting eruption centres by radial linear alignments and MMVC margin by polygonal alignment of linear segments.

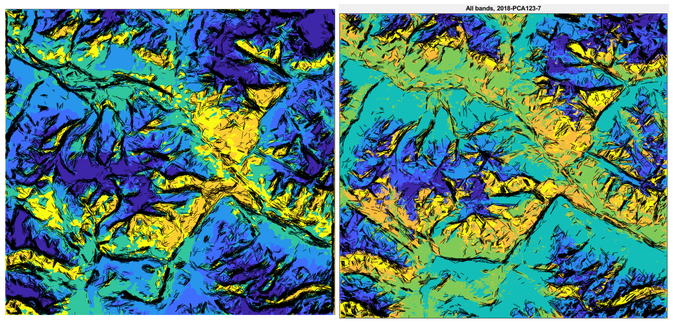


Fig. 7 Left: Thermal feature classification results of TIR images (Table 1) overlain with extracted linear segments. PCA was used to reduce dimension and K-means clustering for classification. Three PCA components (1,2,4) were utilized to represent the spatial variation of land surface thermal (solar radiation) and geothermal energies. This TIR feature classification from multi-season TIR images has a high correlation with LST (Fig, 9), and shows more pertinent geothermal related features than that from a single multi-spectral acquisition. Right: Feature classification map of the 20181019 single multi-spectral data set, showing different categories of feature as feature classes. Similarity to the TIR indicates the common ground in thermal characteristics, while differences are reflection of distinct physical properties of the land surface in visible and NIR-SWIR wavelengths.

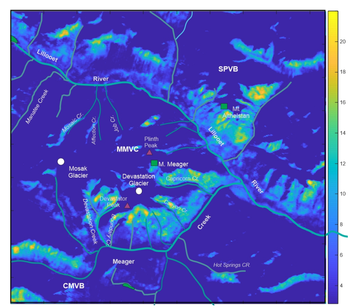


Fig. 9 Geothermal Heat Flux (GHF) components of LST shows temperature anomalies that may be associated with geothermal resources. Methods calculating GHF component is referred to Chen et al (material submitted for publication).

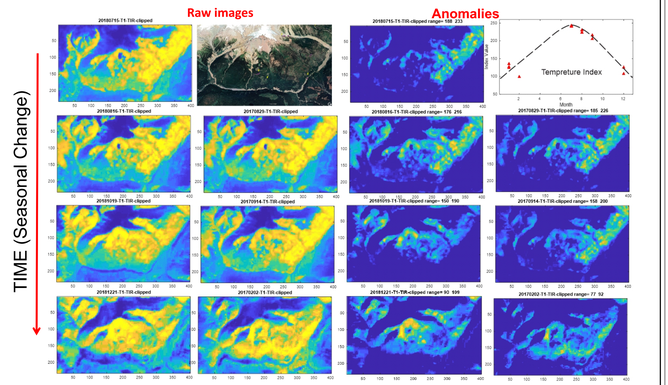


Fig. 10. Thermal infrared (TIR) images from different seasons and years show distinct characteristics and contain information useful for geothermal anomaly interpretation. Spatially, thermal anomalies occur commonly in areas either containing hot springs and swarms of groundwater seep, or near newly exposed hot bedrock due to landslide or other surface geological processes. Thermal anomalies in the former case are easily observable in winter when the temperature contrast of warm water from seeps and hot springs and the surrounding area are largest, and spread out in a wider area. Near newly exposed hot bedrock, the thermal anomalous spots are persistent year around, and occur mostly in the southern MMVC. Major thermal anomaly often shows a sharp linear boundary with the primary anomaly trends striking NE-SW that are intersect with secondary NW and EW striking anomalies.

## Conclusions

Various features from Landsat 8 images were extracted and presented in different forms. Attempts were made to link the observed anomalies to known shallow temperature anomalies, identified fractured/faulted zones in bedrock, and surface indications of groundwater circulation. We have the following observations:

A) Major lineaments are in a good accordance geographically with field geophysical survey inferred faults (Fig. 9);

B) Linear features from images of specific spectral ranges differ, and vary spatially. Along the margin of MMVC, lineaments appear to be circular, separating the complex from the surrounding areas. Radial lineament clusters are found common associated with volcanic eruption centres within MMVC (Figs 5-6). TIR based lineaments are associated with surface and subsurface(?) thermal boundaries, while lineaments from full multi-spectral bands seem to be comprehensive, but more resentative of surface processes;

C) Major LST anomalies have sharp linear boundaries (Figs. 7-10), and NE and NW trends dominate;

D) Thermal anomalies change with time and vary spatially. Two types of surface thermal anomalies might be related to geothermal energy resources: a) persistent high thermal anomalies year around on recent exposed volcanic and intrusive bed-rocks in south facing cliffs in the southern MMVC; and b) narrow linear thermal anomalous zones along certain segments of boundary faults in the MMVC margin associated with hot-spring and water seep swarms (Figs 8-10). The second is more apparent in winter season.

## Acknowledgments

This is an output of Geoscience for New Energy Supply Program of Natural Resources Canada. NRCan's Emerging Renewable Power Program, Office of Energy Research and Development and Geoscience BC provided funding for this study. The Landsat 8 images courtesy of the U.S. Geological Survey.

## References

Darge, YM., Hailu,BT., Muluneh, AA., and Kidane, T., 2019. Detection of geothermal anomalies using Landsat 8 TIRS data in Tulu Moye geothermal prospect, Main Ethiopian Rift, International Journal of Applied Earth Observation and Geoinformation, Volume 74, February 2019, Pages 16-26

Fairbank; B. D. Openshaw; R. E. Souther, J. G. and Stauder, J, J., 1981, Meager Creek geothermal project: an exploration case study, Geothermal Resources Council Bulletin July 1981, p3-7.

GeothermamEx Inc., 2004. Report on the south meager geothermal resource British Columbia, Canada, for Western Geopower Corp. 156p.

Jessop, A.M. 2008, Review of National Geothermal Energy Program, Phase 2 – geothermal potential of the Cordillera. Geological Survey of Canada, Open File 5906, 86 pages.

Lewis, J.F., and Souther, J.G., 1978, Meager Mt., B.C.-Possible Geothermal Energy Resource: EMR, Earth Physics Branch, Geothermal Series No. 9, Ottawa, 17 pp.

Qin, Q., Zhang, N., Nan,P., and Chai, L., 2011. Geothermal area detection using Landsat ETM+ thermal infrared data and its mechanistic analysis—A case study in Tengchong, China, International Journal of Applied Earth Observation and Geoinformation 13 (2011) 552–559.

Stewart, M.L.2002. Dacite block and ash avalanche hazards in mountainous terrain: 2360 yr. B.P. eruption of Mount Meager, British Columbia. M.Sc. Thesis, The University of British Columbia.

[1]Geological Survey of Canada, 3303-33rd Street N.W., Calgary, Alberta

For more information, please contact Z. Chen (zhuoheng.chen@nrcan-rncan.gc.ca).



Permanent link: https://doi.org/10.4095/330008

This publication is available for free download through GEOSCAN (https://geoscan.nrcan.gc.ca/).

OPEN FILE DOSSIER PUBLIC 8882 GEOLOGICAL SURVEY OF CANADA COMMISSION GÉOLOGIQUE DU CANADA 2022

Publications in this series have not been edited; they are released as submitted by the author.

Les publications de cette série ne sont pas révisées; elles sont publiées telles que soumises par l'auteur.

ISSN 2816-7155
ISBN 978-0-660-44153-5
Catalogue No. M183-2/8882E-PDF

**Recommended citation**
Chen, Z., Grasby, S.E., Deblonde, C., and Liu, X., 2022, AI-enabled remote sensing data interpretation for geothermal resource evaluation as applied to the Mount Meager geothermal prospective area, British Columbia; Geological Survey of Canada, Open File 8882, 1 poster. https://doi.org/10.4095/330008

Natural Resources Canada | Ressources naturelles Canada

Canada